Ferroelectric $BaTaO_2N$ perovskite — Towards structure-property relationship study on high-quality crystals and ceramics prepared with the aid of liquid phase

Akira Hosono[1,*], Yuji Masubuchi[2,*], Mikio Higuchi[2], and Shinichi Kikkawa[2]

Affiliations;
[1] Graduate School of Chemical Sciences and Engineering, Hokkaido University, N13 W8, Kita-ku, Sapporo 060-8628, Japan
[2] Faculty of Engineering, Hokkaido University, N13 W8, Kita-ku, Sapporo 060-8628, Japan

Corresponding authors;
*Akira Hosono; E-mail: ezohakitaguniah@gmail.com
*Yuji Masubuchi; E-mail: yuji-mas@eng.hokudai.ac.jp

Abstract

The ternary metal oxynitride compound, perovskite-type $BaTaO_2N$, has been a subject of interest for solid-state physicists and chemists. The notable dielectric property has been reported in a centrosymmetric average structure although the anisotropic anion configuration is preferable in *cis*-TaO_4N_2 octahedra around Ta^{5+} with d^0 electron state. Either single crystals or sintered ceramics in high quality is necessary to clarify the puzzle between the structure and property. Thin film studies are sometimes misleading and confusing. This report reviews the preparation of $BaTaO_2N$ in high quality from the viewpoints of its crystal growth in a liquid phase, sintering in a thick ceramic form, and low-temperature and short time sintering with a liquid phase additive to obtain the high-

quality samples for investigation of the structure-dielectric property relationship.

Keywords: Perovskite-type oxynitride; dielectric; single crystal; ceramics

1. Introduction

Over the last 40 years, a variety of oxynitride compounds with perovskite-type crystal structure have been synthesized. Many examples, such as AETaO$_2$N (AE = Ca, Sr, Ba), AENbO$_2$N, LnTaON$_2$ (Ln = lanthanoid), LnTiO$_2$N, NdVO$_2$N, non-stoichiometric compounds, SrMo(O,N)$_3$, BaW(O,N)$_3$, BaTi(O,N,□)$_3$, where □ is anion vacancy, and a series of Ruddlesden-Popper-type layered perovskites have been reported [1-20]. The powder synthesis of one typical material, BaTaO$_2$N, was firstly reported in 1986 [21]. It took a little longer for the potential of this material as a dielectric material to be revealed because its space group had long been considered to be centrosymmetric $Pm\bar{3}m$ [3]. The local crystal structure of BaTaO$_2$N was furtherly characterized using infrared spectroscopy in 1995 [22]. Some deviation from the centrosymmetric cubic perovskite was observed in a presence of several unattributable peaks but there was no evidence of a soft mode in BaTaO$_2$N polycrystalline pellet.

In 2004, unusually large relative dielectric constant values of BaTaO$_2$N ($\varepsilon_r \approx$ 4600) and SrTaO$_2$N ($\varepsilon_r \approx 3000$) over the temperature range of 180–300 K were reported

for their powder compacts annealed at 1050 °C under ammonia flow. Its relative density (RD) was approximately 55% [23]. However, the centrosymmetric space groups of these materials ($Pm\bar{3}m$ for $BaTaO_2N$ and $I4/mcm$ for $SrTaO_2N$) are contradictory to such large dielectric constant values. Theoretical and crystallographic studies were undertaken to obtain a consistent explanation of polar crystal structures. Local crystallographic anisotropy due to a *cis*-type nitrogen configuration in TaO_4N_2 octahedra has been one important factor to introduce spontaneous polarization into oxynitride perovskites [6,14,24-31]. The local structure of $BaTaO_2N$ examined using transmission electron microscopy (TEM), extended X-ray absorption fine structure, and neutron pair distribution functions suggested several different distances in Ta-O and Ta-N respective bonds [24-26]. These results suggested that each Ta atom is slightly displaced in one direction from its average centrosymmetric position in the cubic perovskite to form one dimensional (linear) polar nano regions (PNRs) [25]. A recent report of secondary harmonic wave generation (SHG) and piezoelectric response from $BaTaO_2N$ microcrystals also supports this hypothesis for the presence of locally non-centrosymmetric structural units in the centrosymmetric average crystal structure [32].

First-principles calculation of structure of $BaTaO_2N$ suggested the local symmetry breaking due to a displacive disorder in Ta-O and Ta-N distances [33]. Density

functional theory (DFT) calculations of both $SrTaO_2N$ and $BaTaO_2N$ with a *cis*-type anion configuration model indicated the formation of helical coil-like polar Ta-N-Ta-N chains with various lengths and directions [27]. In relation to these locally distorted structure models, relaxor-like ferroelectric properties in these oxynitride perovskites were expected. Additional theoretical investigations on each crystal structure of the oxynitride perovskites have been conducted by several independent researchers. Structural optimizations of $CaTaO_2N$, $SrTaO_2N$, and $BaTaO_2N$ were performed using total-energy calculations and phonon-computations [28]. It should be noted that all the oxynitrides were determined to be stable in the orthorhombic *Pnma* space group, unlike their previous powder neutron and X-ray diffraction (XRD) results where centrosymmetric models *I*4/*mcm* for $SrTaO_2N$ and $Pm\bar{3}m$ for $BaTaO_2N$ were assumed [3,4,23]. Further structural optimization for $BaTaO_2N$ indicated that the most favorable space group is non-centrosymmetric $Pmc2_1$ [28], which is consistent with the observation of ferroelectricity in $BaTaO_2N$ crystals, as discussed in the next section [32]. This result has been extended to a series of oxynitride perovskites, such as $LnTaON_2$ (*Ln* = La, Ce, Pr) and $CaTaO_2N$ [29]. However, it is challenging to detect a polar phase of oxynitride perovskites because each domain is too small to induce the diffraction of irradiated beams. Therefore, profile refinements of powder diffraction data tend to converge to averaged high-symmetry space

groups.

Concurrently with crystal structure investigations, many experimental trials were performed to fabricate dense ceramics and thin films to confirm the dielectric properties, as mainly reviewed for $SrTaO_2N$ [34]. However, there had been a number of technical problems to be solved to unambiguously confirm $BaTaO_2N$ as a ferroelectric material, due to difficulty in sintering while maintaining its stoichiometry. There has been much less the fabrication of single crystals than the ceramics. The main difficulty in obtaining dense oxynitride ceramics and single crystals is their thermal instability. The decomposition behavior of $BaTaO_2N$ is strongly dependent on the heating atmosphere, as depicted in the thermogravimetry (TG) curves of Figure 1 [35]. $BaTaO_2N$ begins to release a part of its nitrogen at approximately 920 °C, and its chemical composition is changed to $BaTaO_2N_{0.85}$ with a nitrogen-deficient perovskite-type structure. The chemical composition was estimated from the oxygen and nitrogen contents measured by oxygen/nitrogen combustion analyzer and the nitrogen deficiency was almost consistent with the weight loss in TG measurement. No oxygen release was detected, and further decomposition was almost suppressed in a nitrogen atmosphere, whereas $BaTaO_2N$ was completely decomposed to a mixture of $Ba_5Ta_4O_{15}$, $BaTa_2O_6$, and Ta_2N under helium flow. Quite similar decomposition behavior was reported for the analogous compound

$SrTaO_2N$ [16,36,37]. A high-pressure nitrogen atmosphere was directly applied to investigate the nitrogen release from the oxynitride perovskites using hot isostatic pressing [38]. A $SrTaO_2N$ powder compact lost some nitrogen at 1400 °C even under 190 MPa of nitrogen to form a nitrogen-deficient perovskite, $SrTaO_2N_{0.7}$, which is similar to the decomposition of $BaTaO_2N$ at ambient pressure. This result indicates the formation of nitrogen-deficient perovskite-type oxynitrides is inevitable during high-temperature heating above 920 °C. For the perovskite-type oxynitride, high-temperature sintering and crystal growth from a melt requires an additional process to recover the nitrogen-loss or, conversely, a low temperature process below the decomposition temperature is required.

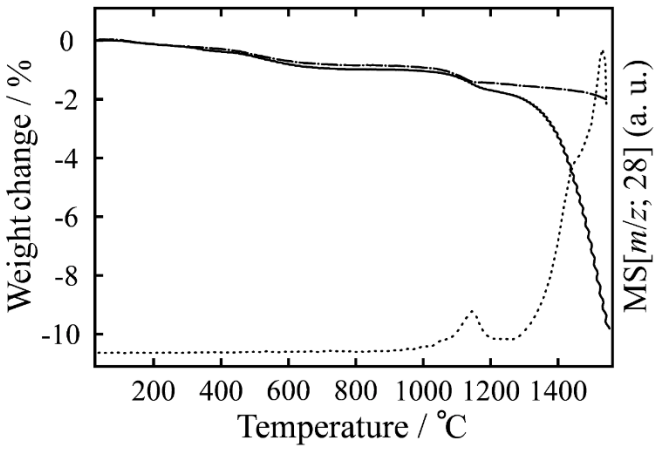

Figure 1. Weight loss of $BaTaO_2N$ oxynitride perovskite powder during heating in a helium (solid line) or nitrogen (dot-dashed line) atmosphere and nitrogen evolution detected by mass spectrometry (helium atmosphere, dashed line). The heating rate in both atmospheres was 20 °C/min [35]. Reproduced with permission from ref. 35. Copyright

2016 Elsevier.

This paper provides a research history of the crystal growth and sintering of $BaTaO_2N$ ferroelectrics with an assistance of a liquid phase towards further investigations on the relation between the crystal structure and dielectric property [32,39,40]. Microcrystal preparation of $BaTaO_2N$ using a low temperature flux is reviewed and its ferroelectric characteristics are discussed. High temperature sintering using a sintering additive followed by nitridation in an ammonia atmosphere is also applied for a thick powder film prepared by electrophoretic deposition (EPD). Sintering at low-temperature with short duration, which was performed in spark plasma sintering (SPS) equipment, is also discussed for the fabrication of a sintered body without nitrogen deficiency.

2. Ferroelectric $BaTaO_2N$ microcrystals

Ferroelectricity does not appear on $BaTaO_2N$ in cubic perovskite-type structure. Local symmetry breaking is needed on the averaged long-range crystal structure induced by the O/N *cis*-type configuration around Ta. The symmetry breaking exhibits ferroelectric and piezoelectectric characteristics in the perovskite-type $BaTaO_2N$. Dense ceramics and single crystal of $BaTaO_2N$ demonstrated polar switching under applying high electrical voltage. In this section, single crystal growth of $BaTaO_2N$ in a $BaCN_2$ flux

is reviewed and ferroelectric behavior of the crystal is discussed.

2. 1 Fluxes for metal nitrides and oxynitride crystals

Solid-state sintering is not applicable to a $BaTaO_2N$ powder compact below 920 °C, at which point it begins to release part of the nitrogen to become an *n*-type semiconductor loosing insulating property. Liquid phases that act as a solvent of $BaTaO_2N$ while maintaining its anion contents would thus be beneficial for its crystal growth or liquid-phase sintering.

There are only a limited number of reports on crystal growth of metal nitrides due to a lack of the knowledge on appropriate fluxes. Na metal and NaN_3 [41,42], Li_3N [43], and Ca_3N_2 [44] are well known fluxes in crystal growth of typical metal nitrides. Melts of Li_3BN_2 and alkaline-earth boron nitrides are fluxes for the productions of hexagonal- and cubic-boron nitride (BN) crystals [45,46]. Flux selection is much more difficult in metal oxynitrides than nitrides. The oxygen/nitrogen molar ratio in target materials needs to be maintained under low oxygen partial pressure atmospheres at high temperature.

Crystal growth trials of transition metal oxynitrides are recently becoming more familiar to solid-state chemists and physicists. Grain growth of relatively large TaON

crystal samples under gigapascal pressure was reported using LiCl flux [47]; however, growth was conducted at 1400 °C, whereby oxygen loss resulted in electrical conductivity. Post-annealing was necessary to compensate for the loss of oxygen, just as in the reports on the high-temperature sintering of $SrTaO_2N$ and $BaTaO_2N$ [35-37]. To maintain the nitrogen stoichiometry of $BaTaO_2N$ and avoid a partial formation to semiconductor, dissolution and recrystallization processes must be conducted at temperatures lower than that of nitrogen loss (920 °C).

Submicron crystals of perovskite-type $BaTaO_2N$ and $LaTiO_2N$ with cubic shape were synthesized using KCl and K_2MoO_4 as fluxes [48,49]. The ammonothermal method has also been employed to grow micron-sized oxynitride perovskite crystallites such as ABO_2N (*A* = Sr, Ba, *B* = Nb, Ta) [50], $LnTaON_2$ (*Ln* = La, Ce, Pr, Nd, Sm, Gd) [51], and $LaNbON_2$ [52]. It should be noted that the residual potassium needs to be removed. Fluxes are more favorable to have similar chemical composition to target materials.

2. 2 Crystal growth of $BaTaO_2N$ in a $BaCN_2$ flux

Metal carbodiimides are ionic crystals composed of metal cations and symmetric $[N=C=N]^{2-}$ anionic unit, which is distinct from asymmetric cyanamide anion $[N–C\equiv N]^{2-}$. Alkaline-earth metal carbodiimides were synthesized by heating their metal

carbonate powder under flowing ammonia at 700–1000 °C [53-56]. Thermochemical experiments in a nitrogen atmosphere indicated the tetragonal phase of $BaCN_2$ has a melting point of 910 °C [53,57], which is slightly below the nitrogen release point of $BaTaO_2N$ (920 °C) [35].

Reddish $BaTaO_2N$ and white $BaCN_2$ powders were mixed and heated in a dry nitrogen atmosphere. Microcrystals of $BaTaO_2N$ were obtained by heating the mixture at 910 °C with successive slow cooling. The size of crystals extracted by nitric acid leaching became larger with an increase in the amount of $BaCN_2$. The largest crystal size was 3.1 μm with 46 mol% $BaCN_2$ flux, as shown by the scanning electron microscopy (SEM) images in Figure 2 [32]. The stoichiometric chemical composition was confirmed on a single grain larger than 2 μm by electron probe micro analysis (EPMA) of $BaTaO_2N$ crystals, combustion analyses, and vivid red color shown in Figure 2(e-2) [2]. Further addition of $BaCN_2$ yielded only small $BaTaO_2N$ crystallites that were less than 100 nm in size because of the full dissolution and successive nucleation of $BaTaO_2N$ from the melt.

High-resolution TEM observation confirmed the cubic or cuboid grains are single crystals of $BaTaO_2N$ perovskite, as shown in the selected area electron diffraction (SAED) pattern in Figure 3(b). Further observation around interface between the $BaTaO_2N$ crystals and solidified $BaCN_2$ flux suggested Ruddlesden-Popper-type

Ba_2TaO_3N acts as a reaction intermediate. The dissolved $BaTaO_2N$ formed Ba-rich matrix with molten $BaCN_2$. And then, $BaTaO_2N$ recrystallized at its outermost surface of the surrounding Ba_2TaO_3N. The process proceeds during the cooling and condensation of solutes due to a flux loss in the heating [32,53].

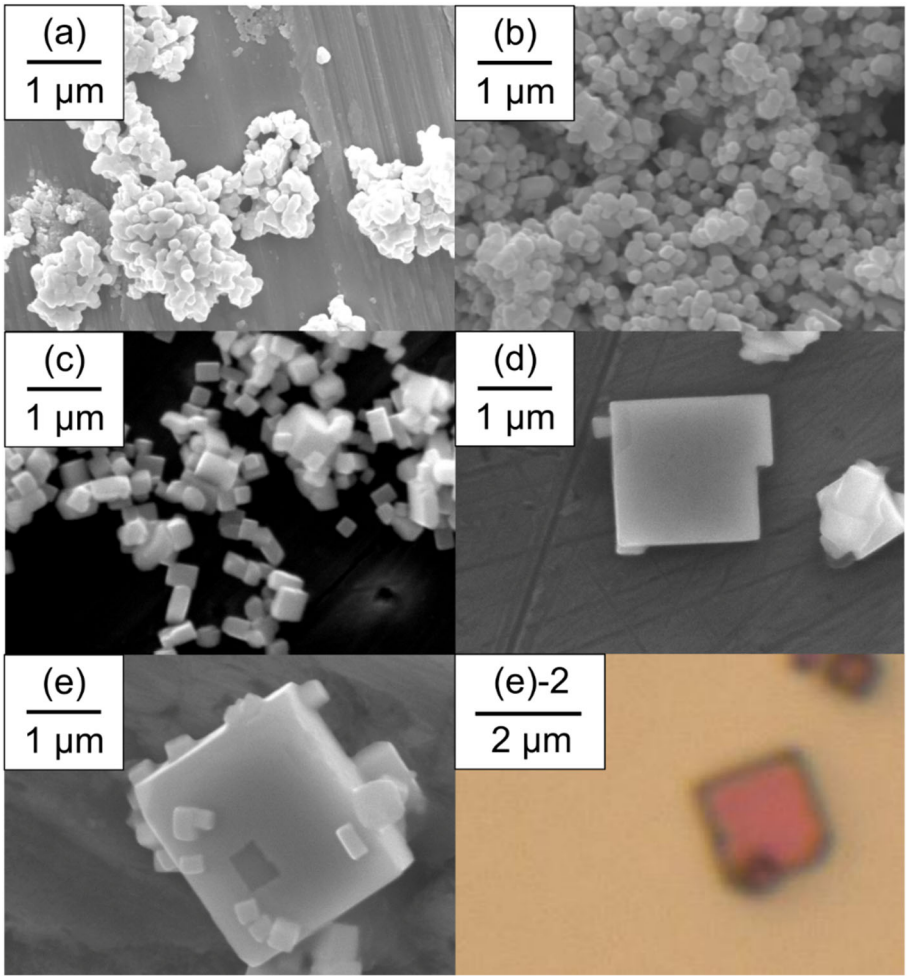

Figure 2. SEM micrographs of $BaTaO_2N$ particles: (a) As-prepared ammonolysis product; (b–e) products generated in the flux at 910 °C for 30 min with 17, 22, 36, and 46 mol% $BaCN_2$, respectively, after cooling at 1.8 °C/h and acid/water washing. [(e)-2] optical micrograph of the product in (e) [32]. Reproduced with permission from ref. 32.

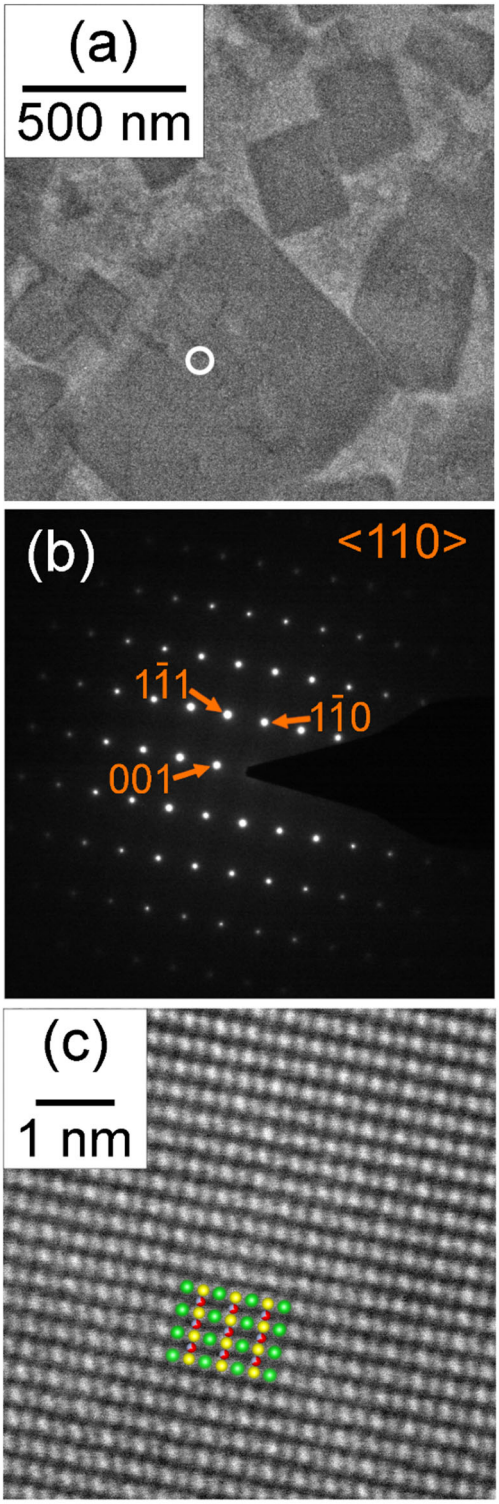

Figure 3. (a) TEM bright-field image of a thin specimen of $BaTaO_2N$ crystals with solidified $BaCN_2$ flux. (b) SAED image of the encircled area in (a). (c) High-magnification high-angle annular dark-field-scanning transmission electron microscopy (HAADF-STEM) image of the area encircled in (a). Green, yellow, and red circles in (c) indicate Ba, Ta, and O/N anions, respectively [32]. The crystal structure model was drawn using the crystallographic imaging software VESTA [58]. Reproduced with permission from ref. 32. Copyright 2019 American Chemical Society.

2. 3 Piezoresponse of $BaTaO_2N$ microcrystals

The piezoelectricity of $BaTaO_2N$ crystals was investigated using piezoresponse force microscopy (PFM) technique [32]. A mono-layered capacitor structure of micron-sized $BaTaO_2N$ crystals was fabricated. A top electrode of Pt is necessary to exclude the negative effect of electrostatic force, which disturbs a clear distinction between intrinsic piezoelectricity of $BaTaO_2N$ crystals and extrinsic effects [59-61]. Electrical insulation was significantly improved in the $BaTaO_2N$ crystals compared to the ceramics that were sintered at high temperature and then nitrided in an ammonia flow [62]. Significant electrical insulation of the crystals made it possible to apply high electrical voltage without current leakage.

Relatively strong electrical field was required for the $BaTaO_2N$ crystals to switch their polarization direction and demonstrate their ferroelectricity [32]. The butterfly-type piezoresponse curve shown in Figure 4(b) and the ferroelectric phase hysteresis graph in Figure 4(c) suggest approximately 250 kV/cm of its coercive electrical field at 120 °C, which may originate from strong covalent bonding due to the presence of nitrogen in the crystal structure. No butterfly-like piezoresponse was obtained at room temperature because the polarization phase alternation was more difficult to change at ambient temperatures [63]. Polarization phase in PNRs is more easily altered at high temperatures as reported in typical relaxor ferroelectrics like $Pb(Mg_{1/3}Nb_{2/3})O_3$ [64]. The polarization phase alternation in $BaTaO_2N$ at high temperature suggests the ferroelectric properties of $BaTaO_2N$ perovskite is conjunction to PNRs. Simple cubic perovskite-like SAED pattern shown in Fig. 3(b) was obtained from the as-grown $BaTaO_2N$ microcrystal, because the non-centrosymmetric polar domain was too small to induce the diffraction and the polarization direction of each domain was randomly distributed in the crystal without polarization. Single crystal of $BaTaO_2N$ after polarization should be used in diffraction experiments to investigate the non-centrosymmetric crystal structure.

In conclusion, $BaTaO_2N$ was confirmed to be a ferroelectric material by PFM measurements of microcrystals. Examinations of their polarization (P)-electrical field (E)

hysteresis and capacitance values for application as dielectrics remains a challenge because of the weak electrical current signal generated via the small electrodes on the microcrystals. Advances of the techniques for crystal growth and a sintering of insulating ceramics are thus urgently required.

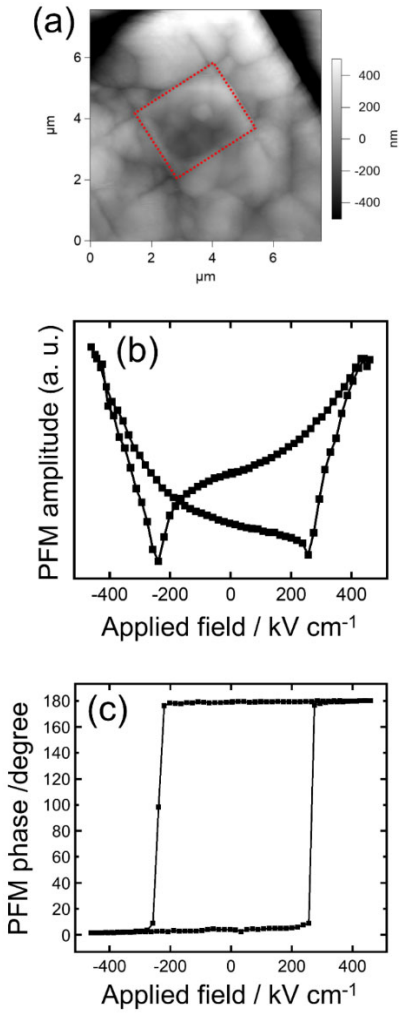

Figure 4. (a) AFM topographical image of a $BaTaO_2N$ crystal (indicated by the dotted red square), (b) piezoresponse amplitude curve obtained at 120 °C, and (c) corresponding ferroelectric phase signal graph [32]. Reproduced with permission from ref. 32. Copyright

2019 American Chemical Society.

3. High temperature sintering and ammonia annealing

PFM measurement using a single crystal of $BaTaO_2N$ confirmed the ferroelectricity and superior electrical insulating properties. Bulk ceramics of $BaTaO_2N$ will enable an evaluation of capacitance and practical applications. However, high-temperature sintering of $BaTaO_2N$ powder compacts results in the formation of semiconductor bulk ceramics that have lost the original insulating properties. In this section, the sintering process of thermally unstable $BaTaO_2N$ is discussed in relation to the use of boron oxide as a sintering additive.

3. 1 High temperature sintering of $BaTaO_2N$

Preliminary sintering studies had been performed without any special care about the thermal release of nitrogen from the oxynitrides. The thermal stability, sinterability, and the electrical and piezoelectric properties of $BaTaO_2N$ polycrystalline ceramics were investigated following the precedent examples of the $SrTaO_2N$ ceramics [16,36,37,65]. To achieve more reliable dielectric constants, several trials were performed to fabricate ceramics with RDs that were higher than those reported by Kim et al. (55%) [23]. Special care to maintain the sintering atmosphere at low oxygen partial pressure is necessary to

operate $BaTaO_2N$ powder at high temperature, because tantalum-containing oxynitride perovskites are easily oxidized to a mixture of their component metal oxides at around 400 °C [66,67]. The decomposition behavior of $BaTaO_2N$ is strongly dependent on the heating atmosphere, as shown by the TG curves in Figure 1 [35].

Solid-state sintering procedures are hardly applicable to metal oxynitrides due to their extremely small diffusion constants; therefore, high-temperature processes and the use of sintering additives are generally necessary to obtain dense ceramics. $BaTaO_2N$ is thermally unstable; therefore, there is a technical difficulty in sintering stoichiometric $BaTaO_2N$ ceramics at high temperatures. A two-step process has been employed that involves high-temperature sintering of nitrogen-deficient $BaTaO_2N_{0.85}$ and subsequent annealing in an ammonia atmosphere to replace the lost nitrogen. To obtain ceramics that maintain the perovskite-type phase requires that $BaTaO_2N$ green-powder compacts be sintered in an inert atmosphere, e.g., pure nitrogen.

To compensate for a slight loss of Ba during high-temperature sintering and avoid the formation of TaN impurities, 2.5–5.0 wt% of $BaCO_3$ was added to $BaTaO_2N$ [35]. During sintering, reddish powder compacts were placed into a BN polycrystalline crucible and held in a pure nitrogen atmosphere at 0.2 MPa. The sample color was changed to black, i.e., changed to a semiconductor, similarly to $SrTaO_2N$, which partially

loses nitrogen to form $SrTaO_2N_{0.7}$ during sintering [16,36,37,65] as the as-sintered ceramics were *n*-type semiconductors because of the partial reduction of Ta^{5+} to Ta^{4+}/Ta^{3+}. Particle necking and densification did not proceed below 1400 °C and the maximum RD value of nitrogen deficient $BaTaO_2N_{0.85}$ was 93.0% [35]. The contribution of a Sr-B-O ternary amorphous phase in the grain boundaries and triple points was recently reported for the sintering of $SrTaO_2N_{0.7}$ with a B_2O_3 sintering additive at 1400 °C [68]. It can thus be inferred that a similar secondary phase could behave as a sintering reagent for $BaTaO_2N_{0.85}$.

The reddish color on the sample was recovered after heating the $BaTaO_2N_{0.85}$ ceramics under ammonia flow at 1000 °C [35]. The homogeneity of annealed ceramics is dependent on the RDs of the $BaTaO_2N_{0.85}$ ceramics. The entire porous bulk (RD ≤ 74.6%) became red, while the interiors of dense samples remained black (semiconductor) because ammonia or related nitriding reagents could not diffuse into the highly densified microstructure [35,62].

3. 2 Thick film of dense $BaTaO_2N$ ceramic sintered with B_2O_3 additive

Dense ceramics of $BaTaO_2N_{0.85}$ were only nitrided in a thin surface layer with a thickness of approximately 10 μm. The surface of the thin layer recovered its nitrogen

content and electrically insulating properties after annealing in ammonia flow. Therefore, thick films of dense oxynitride perovskite ceramic with several tens of micrometers in thickness are expected to achieve both high RD and fully nitridation even after long-term annealing in ammonia. EPD was employed to fabricate thin films of ceramic powder compacts from a colloidal suspension [69,70]. The thickness and microstructure of the powder compacts can be controlled by tuning the deposition conditions, such as the suspension concentration, deposition time, and applied voltage. Powder compacts with a thickness of approximately 100 μm were fabricated from a mixture of $BaTaO_2N$ and a $BaCO_3$ additive using the EPD method. The $BaCO_3$ additive compensates for the small amount of Ba loss that occurs during high-temperature sintering [35]. The powder compacts were placed in an alumina crucible with/without a small amount of B_2O_3 powder additive located in the crucible separate from the powder compacts and then sintered at 1400 °C for 4 h in a N_2 atmosphere at 0.2 MPa. B_2O_3 has been reported as a sintering additive together with $SrCO_3$ for $SrTaO_2N$ to form a Sr-B-O liquid phase during sintering [68]. The effect of the B_2O_3 additive on the sintering of $BaTaO_2N/BaCO_3$ was also investigated by the supply of B_2O_3 to the powder compacts via the vapor phase. The sintered thick films of the $BaTaO_2N_{0.85}$ were black in color and electrically conducting due to the nitrogen loss during high-temperature sintering. To recover the nitrogen content

and electrical insulating properties, the sintered ceramics were subsequently annealed at 950 °C for 100 hours in a NH_3 flow of 100 mL/min.

A single-phase perovskite structure was observed for the ceramic sintered without B_2O_3, and a few secondary phases also appeared for the product sintered with the B_2O_3 additive. The B_2O_3 reacted with a small amount of Ba in the powder compact and Ta-rich impurity phases appeared in the sintered ceramic. Sintering of $SrTaO_2N$ with B_2O_3 also formed nitrogen deficient $SrTaO_2N_{0.75}$ contaminated with $TaO_{0.9}$ [68]. SEM images of the fracture surfaces of the sintered ceramic show a dense microstructure for the product sintered with B_2O_3 (Figure 5(a)). In contrast, the ceramic sintered without B_2O_3 was porous (Figure 5(b)), but the grain size was larger than that sintered with B_2O_3. The RD values for $BaTaO_2N$ sintered with and without the B_2O_3 additive were 92% and 78%, respectively. The improved sinterability could be understood by a formation of barium borate liquid phase [71], similarly to the case of $SrTaO_2N$ sintering with B_2O_3 [68]. The smaller grains obtained by sintering with B_2O_3 resulted from sintering with a small amount of liquid phase and for a short duration, before reaching the grain growth step in the liquid-phase sintering process. Grains larger than 1 μm were formed together with small grains by an increase in the sintering time from 4 to 8 h or by increase in the temperature to 1420 °C. On the other hand, sintering without B_2O_3 corresponded to solid-

phase sintering and grain growth was accelerated by nitrogen deficiency to form large grains. The B_2O_3 additive improved the sintering of $BaTaO_2N$ similar to the case in $SrTaO_2N$.

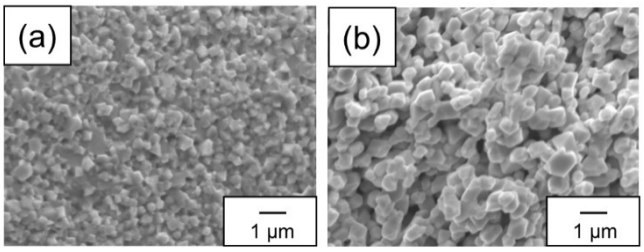

Figure 5. SEM images of fracture surfaces of sintered $BaTaO_2N$ ceramics at 1400 °C for 4 h (a) with B_2O_3 and (b) without B_2O_3. Reproduced with permission from ref. 39. Copyright 2023 Elsevier.

The thick ceramic film sintered at 1400 °C for 4 h with the B_2O_3 additive was annealed in ammonia flow at 950 °C for long duration to compensate for the nitrogen deficiency that developed during the high-temperature sintering. Sample color gradually changed from black to red with increasing the annealing time and the nitrided area extended from the outer surface to the interior as shown in Figure 6. Full nitridation was confirmed by the red color of the sintered product after annealing for 100 h, as shown in Fig. 6(d), which was almost the same color as the green powder compact (Fig. 6(a)). Recovery to the single phase of $BaTaO_2N$ perovskite was also verified by XRD

measurement.

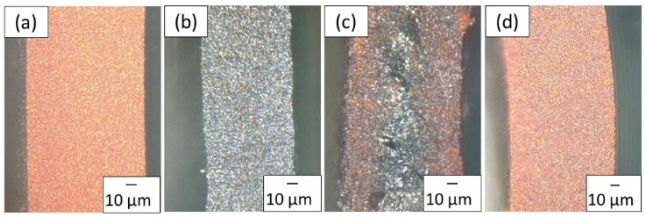

Figure 6. Optical images of cross sections (a) $BaTaO_2N$ powder compact sintered with B_2O_3, and the resultant ceramic after annealing in ammonia flow at 950 °C for (b) 0 h, (c) 60 h, and (d) 100 h. Reproduced with permission from ref. 39. Copyright 2023 Elsevier.

3.3 Dielectric properties of the post-ammonolysis products

The dielectric properties of $BaTaO_2N$ ceramics sintered at 1400 °C for 4 h after nitridations at 950 °C for 0, 60 and 100 h are shown in Figure 7. Nitrogen-deficient $BaTaO_2N_{0.85}$ ceramics without a subsequent nitridation treatment show large relative dielectric constants above 30,000 with large dielectric loss values of 0.6-1. Both the large dielectric constant and loss can be explained by the semiconducting nature of the black sintered ceramic. After nitridation for 60 h, only the surface part of the thick ceramic was nitrided to recover the original red color, as shown in Figure 6(c). The dielectric constant decreased to values of several hundred, and the dielectric loss also decreased but was greater than 0.1. In previous research, the large dielectric constant was determined to

originate from residual semiconducting parts that were not fully nitrided due to the dense bulk structure [35]. The fully nitrided sample with a red interior as shown in Figure 6(d), exhibited dielectric constants of 530-320 at 1.2×10^2-10^6 Hz with tanδ values of 0.15-0.05. These dielectric constants were larger and the dielectric losses were lower than those for bulk ceramics (ε_r = 300 and tanδ = 0.06 at 10^5 Hz) with an RD of 73% [35]. The bulk ceramic with an RD of 73% was readily nitrided due to its porous structure, although some residual semiconducting material may possibly remain after the nitridation for a short duration. The temperature dependence of the dielectric properties is shown in Figure 7(b). An almost flat dependence was observed on the dielectric constant below 250 °C and the dielectric loss was maintained below 0.05. The slightly enhanced dielectric constant above 300 °C may be related to the semiconducting nature of the $BaTaO_2N$ at high temperature. There is no clear trace of a phase transition of the $BaTaO_2N$ ceramics with respect to the temperature, which indicates the ferroelectric characteristics remain up to 300 °C.

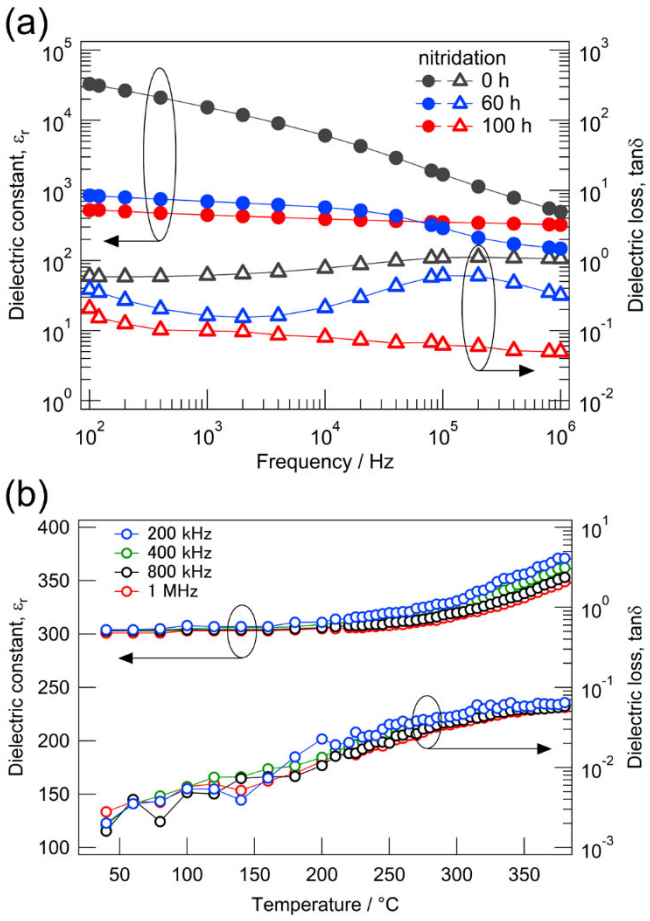

Figure. 7 (a) Frequency dependence of dielectric constants, ε_r, and dielectric loss, tanδ, for ceramics sintered at 1400 °C and annealed in ammonia at 950 °C. (b) Temperature dependence of ε_r, and dielectric loss, tanδ, for the dense ceramics annealed in ammonia at 950 °C for 100 h. (a) was reproduced with permission from ref. 39. Copyright 2023 Elsevier.

4 Sintering of $BaTaO_2N$ using a molten $BaCN_2$ additive in SPS equipment

An ordinary sintering of $BaTaO_2N$ at high temperature fabricated $BaTaO_2N_{0.85}$

dense ceramics with some nitrogen deficiencies. Both original nitrogen content and electrical insulation were recovered only on the ceramic surface as mentioned in section 3.1 and in the thick film as described in section 3.2. However long duration of the post-ammonolysis is required to obtain stoichiometric ceramic products. A $BaCN_2$ melt is used as a flux for the crystal growth of $BaTaO_2N$ below 910 °C, which is slightly below the decomposition temperature. In this section, rapid sintering of $BaTaO_2N$ in low-temperature is discussed by using SPS equipment with a corporation of $BaCN_2$ melt as a sintering aid. Liquid phase sintering mechanism is investigated in relation to the amount of additive.

4. 1 Liquid phase sintering using SPS equipment

Direct sintering of $BaTaO_2N$ ceramics without nitrogen loss is desired to simplify sample preparation to keep the electrical insulation properties compared to the high-temperature sintered product [35,39]. A $BaCN_2$ melt was useful to obtain polycrystalline $BaTaO_2N$ ceramics in SPS equipment for short-term sintering under pressure to avoid the thermal decomposition of $BaTaO_2N$ [40,72-76]. Simple SPS process has also been attempted for $LaTiO_2N$ oxynitride perovskite in a nitrogen atmosphere at 1250–1400 °C [77]. The products were black dense ceramics suggesting that they were

electrical conductive, and the perovskite-type phase was partially decomposed to a mixture of La_2O_3 and TiN. They were not stoichiometric $LaTiO_2N$ and contaminated with their decomposition products. It is most probable that $LaTiO_2N$ itself was not sintered, but that by-products after phase decomposition or a perovskite with high anion deficiency assisted the bulk densification. Additive sintering using a flux is a sensible strategy to lower the sintering temperature and shorten the densification time to overcome the difficulties.

Powder mixtures of $BaTaO_2N$ and 0–20 wt% of $BaCN_2$ were sintered into a 1 mm-thick and 10 mm diameter disk using an SPS equipment. Prior to sintering, additive-free $BaTaO_2N$ mother powder was placed between the $BaTaO_2N/BaCN_2$ mixed powder compact and the carbon die to avoid carbon contamination via molten $BaCN_2$. Uniaxial mechanical pressure was applied to the samples up to 100 MPa and the carbon die was then heated to approximately 900 °C at a rate of 200 °C/min and held for 1–10 min under a nitrogen atmosphere.

All the ceramic products were red in color, which implies a negligible amount of nitrogen deficiency. No densification was observed for the additive-free $BaTaO_2N$ powder. The powder mixtures containing some amount of $BaCN_2$ were rapidly densified to RDs higher than 66.5%. The effects of the amount of $BaCN_2$, the applied pressure, and

the time held at 900 °C on the RD values are shown in Figures 8(a) and 8(b). The $BaCN_2$ additive is obviously effective for rapid densification compared to high-temperature ordinary sintering that forms nitrogen-deficient $BaTaO_2N_{0.85}$.

The samples sintered with 7 wt% $BaCN_2$ tended to show relatively low RD values as shown in Figure 8. Systematic change in RD was observed only on the sintering with 5 wt% $BaCN_2$. The solid particles were closer to each other because there was not too much molten $BaCN_2$. In this case the ceramic products become a little denser with a help of bulk diffusion through the flux. Too much amount of the $BaCN_2$ flux does not enhance the densification. Excess flux run out from the mixture to the powder bed. Some penetration of molten $BaCN_2$ into the additive-free $BaTaO_2N$ powder beds was detected by analysis of the Ba/Ta molar ratios after SPS.

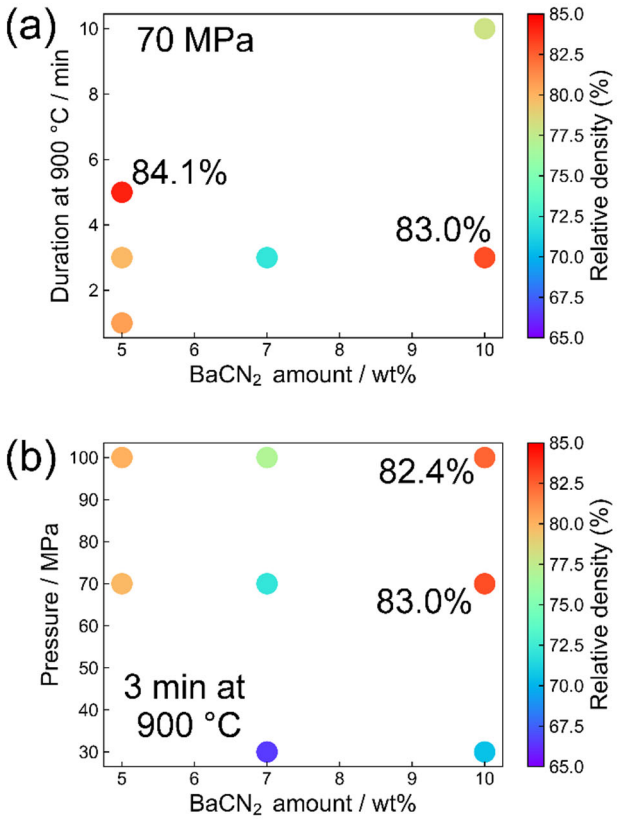

Figure 8. Color map of the RDs of $BaTaO_2N$ ceramics as a function of (a) time held at 900 ℃ and the amount of $BaCN_2$ additive sintered at 70 MPa pressure, and (b) applied uniaxial pressure with the amount of $BaCN_2$ additive sintered at 900 °C of 3 min. The plotted data are for the samples with stoichiometric nitrogen contents.

The effect of the applied mechanical pressure was also examined, and the results are shown in Figure 8(b). The RD values increased under pressure higher than 30 MPa. Molten $BaCN_2$ infiltrated between the $BaTaO_2N$ particles to wet their particle surfaces under mechanical pressure. The RD values did not increase furthermore above 70 MPa,

because an excess amount of molten $BaCN_2$ was removed from the main $BaTaO_2N/BaCN_2$ powder compact to the upper and lower $BaTaO_2N$ powder beds under excessively high pressure. The maximum RD value of the stoichiometric $BaTaO_2N$ ceramics was 84.1%, which was obtained using 5 wt% $BaCN_2$ and a pressure of 70 MPa at 900 °C for 5 min.

4. 2 Sintering mechanism of $BaTaO_2N$ with molten $BaCN_2$

The main crystalline phase in the SPS ceramics was perovskite-type $BaTaO_2N$ and Ba-rich Ruddlesden-Popper-type Ba_2TaO_3N appeared as a secondary phase similar to the crystal growth of $BaTaO_2N$ with $BaCN_2$ [32]. Material diffusion is assisted by chemical reactions in which the perovskite oxynitride dissolves and recrystallizes from the molten $BaCN_2$. Figure 9(a) shows a TEM bright-field image of a thin ceramic specimen with an RD of 80.7% obtained in SPS equipment and the primary particle size of as-prepared $BaTaO_2N$ powder is shown in Figure 9(d). Grains in the ceramics are connected via thin boundaries and some voids are observed in the microstructure. Large pores in the ceramics are present (Fig. 9(a)) probably because the packing of starting powder was insufficient. Energy dispersive X-ray spectroscopy (EDS) compositional analysis was conducted at several points across a grain boundary, as shown in the

HAADF-STEM image (Figure 9(b)). The Ba/Ta molar ratio gradually increased from the grain interior to the exterior and the maximum value was at the triple point (point 4 in Figure 9(b)). Molten $BaCN_2$ spread out into a narrow grain boundary area due to the mechanical pressure and wetted the $BaTaO_2N$ grain surface forming Ba-rich Ruddlesden-Popper phase. The $BaCN_2$ flux is concentrated in the triple points of solidified $BaTaO_2N$ grains. Such Ba-rich constituents can sometimes be confined in the triple points of the grown $BaTaO_2N$ grains as shown in Figure 9(c).

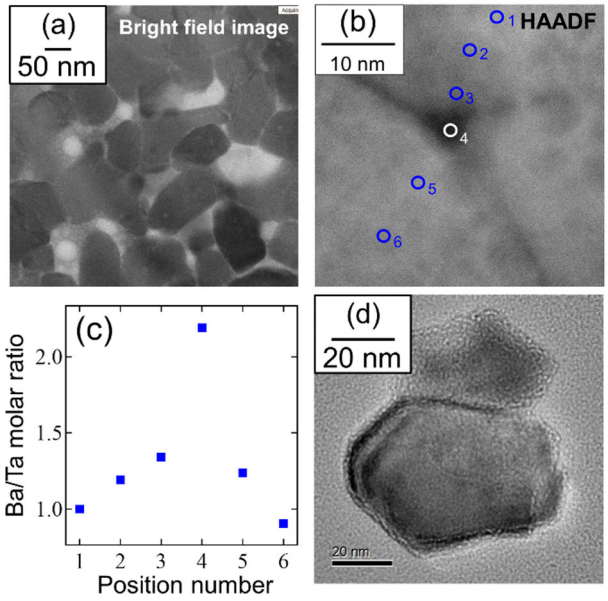

Figure 9. (a) TEM bright-field and (b) HAADF-STEM images of a $BaTaO_2N$ ceramic specimen with an RD of 80.7%. (c) Ba/Ta molar ratios observed using EDS at several points indicated in (b). (d) Bright-field image of the as-prepared $BaTaO_2N$ particles obtained by the ammonolysis [40]. Reproduced with permission from ref. 40. Copyright 2020 Elsevier.

4. 3 Electrical properties of the $BaTaO_2N$ ceramics prepared in SPS equipment

The electrical properties of the $BaTaO_2N$ ceramic sample wih an RD of 79.8% were examined at room temperature over a frequency range of 10^2–10^6 Hz. Figure 10(a) shows a Cole-Cole plot with only a small part of a giant arc, which suggests electrically insulating characteristics, even without post-ammonolysis. Figure 10(b) shows a relative dielectric constant ε_r of 320 and a dielectric loss tanδ of 0.04 at 10^5Hz, which are comparable with the best values reported for a post-annealed ceramics thick film with an RD of 89% sintered at high temperature (ε_r = 300 and tanδ = 0.04) [39]. These values for dielectric property suggest that partial nitrogen loss did not occur in the present sintering at 900 °C. The densification was possible below the temperature for nitrogen release from $BaTaO_2N$ and around the melting point of $BaCN_2$.

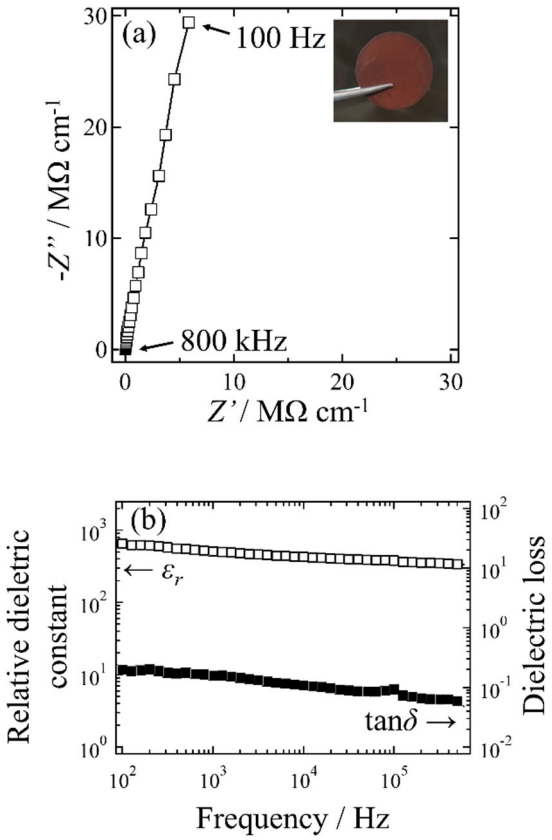

Figure 10. (a) Cole-Cole impedance plots and (b) dielectric properties of a $BaTaO_2N$ ceramic (RD = 79.8%) as a function of frequency at room temperature. The inset in (a) shows a photograph of the polished ceramic surface [40]. Reproduced with permission from ref. 40. Copyright 2020 Elsevier.

In summary, $BaTaO_2N$ powder was sintered at the lowest temperature (approximately 900 °C) among those sintering studies, using a $BaCN_2$ additive under mechanical pressure in SPS equipment to avoid partial nitrogen loss. $BaTaO_2N$ grains were sintered each other through their dissolution and precipitation around their surfaces

in the $BaCN_2$ melt. A minor reaction product, Ba-rich Ruddlesden-Popper-type Ba_2TaO_3N, was present in the grain boundaries and triple points of the ceramics. Rapid heating and cooling processes in an SPS furnace were also effective to avoid partial nitrogen loss from $BaTaO_2N$ crystal lattice. A maximum RD of 84.1% was observed for the $BaTaO_2N$ ceramic with the original nitrogen content maintained. Further increase in the RD could be achieved by improvement of the starting $BaTaO_2N$ powder contacts through a change in the morphology or through the use of an alternative flux with a lower melting point to allow for longer sample heating times for densification.

5. Conclusions and Future Outlook

During the last decade, perovskite-type $BaTaO_2N$ has attracted much attention in solid state chemistry and physics. It was interesting as photocatalyst, lead-free pigment and dielectric materials. High quality sample was necessary to study its ferroelectricity in detail especially in the relation to crystal structure. Flux growth using $BaCN_2$ melt has been applied to $BaTaO_2N$ and several micron-sized crystallites were produced without loss of the electrical insulation properties. Clear evidence of ferroelectricity with large coercivity was also obtained for small $BaTaO_2N$ single crystals.

Dense ceramic thick films of nitrogen-deficient $BaTaO_2N_{0.85}$ were obtained by

high-temperature sintering of the compacts with a B_2O_3 additive by liquid-phase sintering. An electrically insulating dense ceramics of $BaTaO_2N$ with RD of 89% after annealing in ammonia showed a small temperature dependence of the dielectric constant of 300 and a dielectric loss below 0.05 up to 250 °C.

Another big advance was attained in low temperature sintering using $BaCN_2$ melt under mechanical pressure in SPS furnace. The $BaTaO_2N$ ceramic products were nitrogen loss-free maintaining the electrical insulation properties. It was possible to evaluate $BaTaO_2N$ ceramics as dielectric materials.

These high-quality products are now making a noticeable progress to study structure-property relation of the ferroelectricity in $BaTaO_2N$ [78]. Its non-centrosymmetric local structure needs to be clarified in the superficially centrosymmetric space group of $BaTaO_2N$. The spontaneous polarization can be estimated in the local structure. When the structure-property relationship is clarified, partial anion replacement will then make a great number of ternary materials to show novel and attractive functions. Authors believe that progress in high-quality processing will bring the well-sophisticated characterization of mixed anion products especially on $BaTaO_2N$ oxynitride perovskite.

Acknowledgments and Grants

The authors are grateful to the following for technical supports and invaluable

discussions: Professor Hisanori Yamane of Tohoku University, Japan for the crystal growth of oxynitrides, Professors Mitsuru Itoh and Shintaro Yasui of the Tokyo Institute of Technology, Japan for piezoelectric measurements of oxynitride crystals, Dr. Tetsuo Uchikoshi and Kento Ishii of the National Institute of Materials Science, Japan for electrophoretic deposition experiments.

We express gratitude to our former colleagues, Dr. S.-K. Sun of Foshan University, China. Valuable experimental results were obtained by our following alumni students: Dr. Y. -R. Zhang, Ms. D. Chen, Mr. D. Habu, Mr. M. Tadaki, Mr. D. Miyamoto, Mr. K. Koyama, and Mr. H. Takeuchi.

This research was partially financed by a Kakenhi Grant-in-Aids for Scientific Research (A) (No. 24245039) from the Japan Society for the Promotion of Science (JSPS) and as a part of the "Nanotechnology Platform" Program of the Japanese Ministry of Education, Culture, Sports, Science and Technology (MEXT) (Grant A-18-HK-00100). AH was supported by a JSPS research fellowship (Grant 19J10301). YM was also supported partly by a JSPS Grant-in-Aid for Scientific Research on Innovative Areas "Mixed anions" (Grant JP16H06439).

References

[1] M. Jansen, H.P. Letschert, Inorganic yellow-red pigments without toxic metals, Nature 404 (2000) 980–982.

[2] R. Aguiar, D. Logvinovich, A. Weidenkaff, A. Rachel, A. Reller, S.G. Ebbinghaus, The vast colour spectrum of ternary metal oxyniride pigments, Dyes Pigment. 76 (2008) 70–75.

[3] F. Pors, R. Marchand, Y. Laurent, Structural study of $BaTaO_2N$ and $BaNbO_2N$ oxynitrided perovskites, Mat. Res. Bull. 23 (1988) 1447–1450.

[4] S.J. Clarke, K.A. Hardstone, C.W. Michie, M.J. Rosseinski, High-temperature synthesis and structures of perovskite and n=1 Ruddlesden-Popper tantalum oxynitrides, Chem. Mater. 14 (2002) 2664–2669.

[5] R. Marchand, F. Pors, Y. Laurent, Novelles perovskites oxynitrures de stoechiometrie ABO_2N (A = Lanthanide, B = Ti) et $ABON_2$ (A = Lanthanide, B = Ta ou Nb)", Ann. Chim. Fr. 16 (1991) 553–560.

[6] D. Habu, Y. Masubuchi, S. Torii, T. Kamiyama, S. Kikkawa, Crystal structure study of dielectric oxynitride perovskites $La_{1-x}Sr_xTiO_{2+x}N_{1-x}$ (x = 0, 0.2), J. Solid State Chem. 237 (2016) 254–257.

[7] G. Tobías, D.B. Porter, O.I. Lebedev, G.V. Tendeloo, J.R. Carvajal, A. Fuertes, Anion

ordering and defect structure in Ruddlesden-Popper strontium niobium oxynitrides, Inorg. Chem. 43 (2004) 8010–8017.
[8] G. Tobías Rossell, A. Fuertes, E. Canadell Casanova, Nuevos oxinitruros laminares de niobio y tántalo y sistemas relacionados : síntesis, cristaloquímica y estructura electrónica. Bellaterra: Universitat Autònoma de Barcelona, 2004. ISBN 8468891444. Tesi doctoral - Universitat Autònoma de Barcelona, https://ddd.uab.cat/record/37099, 2004 (accessed 5 January 2023).
[9] Y. Masubuchi, T. Hata, T. Motohashi, S. Kikkawa, Synthesis and crystal structure of K_2NiF_4-type novel $Gd_{1+x}Ca_{1-x}AlO_{4-x}N_x$ oxynitrides, J. Alloy Compds. 582 (2014) 823–826.
[10] R. Marchand, Y. Laurent, J. Guyader, P. L'Haridon, P. Verdier, Nitrides and Oxynitrides: Preparation, Crystal Chemistry and Properties, J. Eur. Ceram. Soc. 8 (1991) 197–213.
[11] F. Chevire, A. Pallu, E. Ray, F. Tessier, Characterization of Nd_2AlO_3N and Sm_2AlO_3N oxynitrides synthesized by carbothermal reduction and nitridation, J. Alloy Compds. 509 (2011) 5839–5842.
[12] G. Liu, The synthesis, structure and characterization of $SrMoO_{2.6}{}^{15}N_{0\ 4}$", J. Alloy Compds. 187 (1992) 145–156.
[13] I. D. Fawcett, K. V. Ramanujachary, M. Greenblatt, Synthesis, structure and Properties of the oxynitrides $SrWO_2N$ and $SrMoO_{2.5}N_{0.5}$", Mat. Res. Bull. 32 (1997) 1565–1570.
[14] J. Oró-Solé, L. Clark, W. Bonin, J. P. Attfield, A. Fuertes, Anion-ordered chains in a d^1 perovskite oxynitride: $NdVO_2N$, Chem. Comm. 49 (2013) 2430–2432.
[15] T. Bräuniger, T. Müller, A. Pampel, H. -P. Abicht, "Study of oxygen-nitrogen replacement in $BaTiO_3$ by ^{14}N solid-state nuclear magnetic resonance", Chem. Mater. 17 (2005) 4114–4117.
[16] D. Chen, D. Habu, Y. Masusbuchi, S. Torii, T. Kamiyama, S. Kikkawa, Partial nitrogen loss in $SrTaO_2N$ and $LaTiO_2N$ oxynitride perovskites, Solid State Sci. 54 (2016) 2–6.
[17] T. Motohashi, Y. Hamade, Y. Masubuchi, T. Takeda, K. Murai, A. Yoshiasa, S. Kikkawa, Structural phase transition in the perovskite-type tantalum oxynitride, $Ca_{1-x}Eu_xTa(O,N)_3$, Mat. Res. Bull. 44 (2009) 1899–1905.
[18] S.J. Clarke, B.P. Guinot, C.W. Michie, M.J.C. Calmont, M.J. Rosseinsky, Oxynitride perovskites: synthesis and structures of $LaZrO_2N$, $NdTiO_2N$, and $LaTiO_2N$ and comparison with oxide perovskites, Chem. Mater. 14 (2002) 288–297.
[19] P. Antoine, R. Assabaa, P. L'Haridon, R. Marchand, Y. Laurent, Transport properties

of the new perovskite-type $LaVO_{3-x}N_x$ oxynitrides, Mat. Sci. Eng. B5 (1989) 43–46.
[20] P. Antoine, R. Marchand, Y. Laurent, On the electrical properties of the perovskites $LnWO_xN_{3-x}$, Mat. Res. Bull. 23 (1988) 953–957.
[21] R. Marchand, F. Pors, Y. Laurent, Elaboration and characterization of new oxynitrides with a perovskite structure, Rev. Int. Hautes Temper. Refract. 23 (1986) 11-15.
[22] X. Gouin, R. Marchand, Y. Laurent, Infrared dielectric response of $BaTaO_2N$, Solid State Commun. 93 (1995) 857–859.
[23] Y.-I. Kim, P.M. Woodward, C.-W. Tai, Characterization of the Structural, Optical, and Dielectric Properties of Oxynitride Perovskites AMO_2N(A = Ba, Sr, Ca ; M = Ta, Nb), Chem. Mater. 16 (2004) 1267–1276.
[24] K. Page, M. W. Stoltzfus, Y. -I. Kim, T. Proffen, P. M. Woodward, A. K. Cheetham, R. Seshadri, Local atomic ordering in $BaTaO_2N$ studied by neutron pair distribution function analysis and density function theory, Chem. Mater. 19 (2007) 4037–4042.
[25] R.L. Withers, Y. Liu, P.M. Woodward, Y.I. Kim, Structurally frustrated polar nanoregions in $BaTaO_2N$ and the relationship between its high dielectric permittivity and that of $BaTiO_3$, App. Phys. Lett. 92 (2008) 102907/1-3.
[26] B. Ravel, Y.I. Kim, P.M. Woodward, C.M. Fang, Role of local disorder in the dielectric response of $BaTaO_2N$, Phys. Rev. B 73 (2006) 184121/1-7.
[27] Y. Hinuma, H. Moriwake, Y. Zhang, T. Motohashi, S. Kikkawa, I. Tanaka, First principles study on relaxor-type ferroelectric behavior without chemical inhomogeneity in $BaTaO_2N$ and $SrTaO_2N$, Chem. Mater. 24 (2012) 4343–4349.
[28] H. Wolff, R. Dronskowski, First-Principles and Molecular-Dynamics Study of Structure and Bonding in Perovskite-Type Oxynitrides ABO_2N (A = Ca, Sr, Ba; B = Ta, Nb), J. Comput. Chem. 29 (2008) 2260–2267.
[29] S.H. Porter, X. Huang, P.M. Woodward, Study of Anion Order/Disorder in $RTaN_2O$ (R = La, Ce, Pr) Perovskite Nitride Oxides, Cryst. Growth Des. 14 (2014) 117–125.
[30] Y.-R. Zhang, T. Motohashi, Y. Masubuchi, S. Kikkawa, Local anionic ordering and anisotropic displacement in dielectric perovskite $SrTaO_2N$, J. Ceram. Soc. Jpn. 119 (2011) 581–586.
[31] M. Yang, J. Oró-Solé, J. A. Rodgers, A. B. Jorge, A. Fuertes, J. P. Attfield, Anion order in perovskite oxynitrides, Nat. Chem. 3 (2011) 47–52.
[32] A. Hosono, Y. Masubuchi, S. Yasui, M. Takesada, T. Endo, M. Higuchi, M. Itoh, S. Kikkawa, Ferroelectric $BaTaO_2N$ Crystals Grown in a $BaCN_2$ Flux, Inorg. Chem. 58 (2019) 16752–16760.
[33] C.M. Fang, G.A. de Wijs, E. Orhan, G. de With, R.A. de Groot, H.T. Hintzen, R.

Marchand, Local structure and electrical properties of $BaTaO_2N$ with perovskite-type structure, J. Phys. Chem. Solids, 64 (2003) 281-286.
[34] Y. Masubuchi, S. -K. Sun, S. Kikkawa, Processing of dielectric oxynitride perovskites for powders, ceramics, compacts and thin films, Dalton Trans. 44 (2015) 10570–10581.
[35] A. Hosono, S.-K. Sun, Y. Masubuchi, S. Kikkawa, Additive sintering and post-ammonolysis of dielectric $BaTaO_2N$ oxynitride perovskite, J. Eur. Ceram. Soc. 36 (2016) 3341–3345.
[36] Y.-R. Zhang, T. Motohashi, Y. Masubuchi, S. Kikkawa, Sintering and Dielectric Properties of Perovskite $SrTaO_2N$ Ceramics, J. Eur. Ceram. Soc. 32 (2012) 1269–1274.
[37] S.-K. Sun, Y.-R. Zhang, Y. Masubuchi, T. Motohashi, S. Kikkawa, Additive sintering, postannealing, and dielectric properties of $SrTaO_2N$, J. Am. Ceram. Soc. 97 (2014) 1023–1027.
[38] A. Hosono, Y. Masubuchi, S. Kikkawa, Sintering behavior of dielectric $SrTaO_2N$ under high pressure of nitrogen, Ceram. Int. 43 (2017) 2737–2742.
[39] H. Takeuchi, D. Miyamoto, Y. Masubuchi, M. Higuchi, K. Ishii, T. Uchikoshi, Preparation of thick dense ceramic films of dielectric $BaTaO_2N$ thorough electrophoretic deposition, Ceram. Int. 49 (2023) 21825–21829.
[40] A. Hosono, M. Inoguchi, Y. Masubuchi, K. Murayama, M. Iha, M. Higuchi, S. Kikkawa, Spark Plasma Sintering of Dielectric $BaTaO_2N$ close to the Melting Point of the $BaCN_2$ Additive, J. Eur. Ceram. Soc. 40 (2020) 2317–2322.
[41] H. Yamane, M. Shimada, S. J. Clarke, F. J. DiSalvo, Preparation of GaN Single Crystals Using a Na Flux, Chem. Mater. 9 (1997) 413–416.
[42] H. Yamane, F. J. DiSalvo, Sodium flux synthesis of nitrides, Prog. Solid State Chem. 51 (2018) 27–40.
[43] G. Wang, J. Jian, W. Yuan, X. Chen, Growth of GaN Single Crystals Using Ca-Li_3N Composite Flux, Cryst. Growth Des. 6 (2006) 1157–1160.
[44] C.O. Dugger, “The synthesis of aluminum nitride single crystals, Mat. Res. Bull. 9 (1974) 331–336.
[45] T. Taniguchi, S. Yamaoka, Spontaneous nucleation of cubic boron nitride single crystal by temperature gradient method under high pressure, J. Cryst. Growth 222 (2001) 549–547.
[46] T. Taniguchi, K. Watanabe, Synthesis of high-purity boron nitride single crystals under high pressure by using Ba-BN solvent, J. Cryst. Growth 303 (2007) 525–529.
[47] K. Ishida, C. Tassel, D. Kato, H. Ubukakta, K. Murayama, T. Murakami, M. Yashima, Y. Higo, Y. Tange, W. A. Phelan, T. M. McQueen, H. Kageyama, Highly Electron-Doped

TaON Single-Crystal Growth by a High-Pressure Flux Method, Inorg. Chem. 61 (2022) 11118–11123.
[48] M. Hojamberdiev, K. Yubuta, J. J. M. Vequizo, A. Yamanaka, S. Oishi, K. Domen, K. Teshima, NH_3-assisted flux growth of cube-like $BaTaO_2N$ submicron crystals in a completely ionized nonaqueous high-temperature solution and their water splitting activity, Cryst. Growth Des. 15 (2015) 4663–4671.
[49] M. Hojamberdiev, A. Yamaguchi, K. Yubuta, S. Oishi, K. Teshima, Fabrication of $La_2Ti_2O_7$ Crystals Using an Alkali-Metal Molibdate Flux Growth Method and Their Nitridability To Form $LaTiO_2N$ Crystals under a High-Temperature NH_3 atmosphere, Inorg. Chem. 54 (2015) 3237–3244.
[50] N. Cordes, T. Bräuniger, W. Schnick, Ammonothermal Synthesis of *EAM*O_2N (*EA* = Sr, Ba; *M* = Nb, Ta) Perovskites and ^{14}N Solid-State NMR Spectroscopic Investigations of *AM*(O,N)$_3$ (*A* = Ca, Sr, Ba, La), Eur. J. Inorg. Chem. 2018 (2018) 5019–5026.
[51] N. Cordes, W. Schnick, Ammonothermal Synthesis of Crystalline Oxonitride Perovskites *Ln*$TaON_2$ (*Ln* = La, Ce, Pr, Nd, Sm, Gd), Chem. Eur. J. 23 (2017) 11410–11415.
[52] C. Izawa, T. Kobayashi, K. Kishida, T. Watanabe, Ammonothermal Synthesis and Photocatalytic Activity of Lower Valence Cation-Doped $LaNbON_2$, Adv. Mat. Sci. Engin. 2014 (2014) 465720/1-5.
[53] A. Hosono, Y. Masubuchi, T. Endo, S. Kikkawa, Molten $BaCN_2$ for the sintering and crystal growth of dielectric oxynitride perovskites $Sr_{1-x}Ba_xTaO_2N$ (x = 0.04 – 0.23), Dalton Trans. 46 (2017) 16837–16844.
[54] A. Perret, A. M. Krawezynski, Recherches sur les cyanamides métalliques, Helv. Chim. Acta 15 (1932) 1009–1022.
[55] S. Nagai, G. Yamaguchi, Studies on Synthesis of Calcium Cyanamide from Calcium Carbonate and Ammonia, I, J. Soc. Chem. Ind. Japan 43 (1940) 219B.
[56] Y. Masubuchi, S. Nishitani, A. Hosono, Y. Kitagawa, J. Ueda, S. Tanabe, H. Yamane, M. Higuchi, and S. Kikkawa, Red-emission over a wide range of wavelengths at various temperatures from tetragonal $BaCN_2$:Eu^{2+}, J. Mater. Chem. C 6 (2018) 6370–6377.
[57] A. Hosono, R. P. Stoffel, Y. Masubuchi, R. Dronskowski, S. Kikkawa, Melting Behavior of Alkaline-Earth Metal Carbodiimides and Their Thermochemistry from First-Principles, Inorg. Chem. 58 (2019) 8938–8942.
[58] K. Momma, F. Izumi, VESTA 3 for three-dimensional visualization of crystal, volumetric and morphology data, J. Appl. Crystallogr. 44 (2011) 1272–1276.
[59] D. Seol, B. Kim, Y. Kim, Non-piezoelectric effects in piezoresonse force microscopy, Curr. Appl. Phys. 17 (2017) 661–674.

[60] N. Faraji, Z. Yan, J. Seidel, Electrical conduction at domain walls in lead titanate ($PbTiO_3$) single crystals, Appl. Phys. Lett. 110 (2017) 213108/1-5.
[61] J. Seidel, L. W. Martin, Q. He, Q. Zhan, Y. -H. Chu, A. Rother, M. E. Hawkridge, P. Maksymovych, P. Yu, M. Gajek, N. Balke, S. V. Kalinin, S. Gemming, F. Wang, G. Catalan, J. F. Scott, N. A. Spaldin, J. Orestein, R. Ramesh, Conduction at domain walls in oxide multiferroics, Nat. Mater. 8 (2009) 229–234.
[62] A. Hosono, Y. Masubuchi, Y. Nagamine, T. Shibahara, S. Kikkawa, Piezoresponse and microstructure of $BaTaO_2N$ ceramics, J. Eur. Ceram. Soc. 38 (2018) 3478–3482.
[63] W.J. Merz, Domain formation and domain wall motions in ferroelectric $BaTiO_3$ single crystals, Phys. Rev., 95 (1954) 690-698.
[64] D. Fu, H. Taniguchi, M. Itoh, S. Koshihara, N. Yamamoto, S. Mori, Relaxor $Pb(Mg_{1/3}Nb_{2/3})O_3$: A ferroelectric with multiple inhomogeneities, Phys. Rev. Lett., 103 (2009) 207601/1-4.
[65] S. Kikkawa, S. -K. Sun, Y. Masubuchi, Y. Nagamine, T. Shibahara, Ferroelectric response induced by *cis*-type anion ordering in $SrTaO_2N$ oxynitride perovskite, Chem. Mater. 28 (2016) 1312–1317.
[66] A. Rachel, S. G. Ebbinghaus, M. Güngerich, P. J. Klar, J. Hanss, A. Weidenkaff, A. Reller, Tantalum and niobium perovskite oxynitrides Synthesis and analysis of the thermal behavior, Thermochimica Acta, 438 (2005) 134 – 143.
[67] R. Aguiar, D. Logvinovich. A. Weidenkaff, A. Reller, S. G. Ebbinghaus, Thermal oxidation of oxynitride perovskites in different atmospheres, Thermochimica Acta 471 (2008) 55 – 60.
[68] Y. Masubuchi, D. Miyamoto, M. Higuchi, B_2O_3 as a new sintering additive for perovskite-type $SrTaO_2N$ oxynitride ceramics, J. Asian Ceram. Soc. 10 (2022) 158 – 164.
[69] P. Sarkar, P. S. Nicholson, Electrophoretic deposition (EPD): mechanisms, kinetics, and application to ceramics. J. Am. Ceram. Soc. 79 (1996) 1987-2002.
[70] F. Tang, T. Uchikoshi, K. Ozawa, Y. Sakka, Effect of polyethyleneimine on the dispersion and electrophoretic deposition of nano-sized titania aqueous suspensions. J. Eur. Ceram. Soc. 26 (2006) 1555-1560.
[71] H. Yu, Q. Chen, Z. Jin, Thermodynamic reassessment of the BaO-B_2O_3 system, J. Phase Equil. 20 (1999) 479–484.
[72] W. Li, E. Olevski, J. McKittrick, A. L. Maximenko, R. M. German, Densification mechanisms of spark plasma sintering: multi-step pressure dilatometry, J. Mater. Sci. 47 (2012) 7036–7046.
[73] R. Chaim, G. Chevallier, A. Weidel, C. Estournés, Grain growth during spark plasma and flash sintering of ceramic nanoparticles: a review, J. Mater. Sci. 53 (2018) 3087–3105.

[74] M.J. Li, L.M. Zhang, Q. Shen, T. Li, M. Q. Yu, Microstructure and properties of spark plasma sintered AlN ceramics, J. Mater. Sci., 41 (2006) 7934–7938.
[75] D. Salamon, Z. Shen, P. Sajgalik, Rapid formation of α-sialon during spark plasma sintering: Its origin and implications, J. Eur. Ceram. Soc. 27 (2007) 2541–2547.
[76] Z. Shen, M. Nygren, Microstructural Prototyping of Ceramics by Kinetic Engineering: Applications of Spark Plasma Sintering, Chem. Rec. 5 (2005) 173–184.
[77] D. Li, W. Li, C. Fasel, J. Shen, R. Riedel, Sinterability of the oxynitride $LaTiO_2N$ with perovskite-type structure, J. Alloys Compds. 586 (2014) 567–573.
[78] Y. Masubuchi, K. Koyama, A. Hosono, M. Tekesada, M. Higuchi, S. Kikkawa, *Cis* TaO_4N_2 octahedral chains extend to 50 nm domains forming an average cubic lattice in $BaTaO_2N$ crystal lattice, in preparation.